BNL-213810-2020-JAAM

Comparison of hafnium dioxide and zirconium dioxide grown by plasma-enhanced atomic layer deposition for the application of electronic materials

X. Xiao, K. Kisslinger

To be published in "Crystals"

February 2020

Center for Functional Nanomaterials

Brookhaven National Laboratory

U.S. Department of Energy

USDOE Office of Science (SC), Basic Energy Sciences (BES) (SC-22)

Notice: This manuscript has been authored by employees of Brookhaven Science Associates, LLC under Contract No. DE-SC0012704 with the U.S. Department of Energy. The publisher by accepting the manuscript for publication acknowledges that the United States Government retains a non-exclusive, paid-up, irrevocable, world-wide license to publish or reproduce the published form of this manuscript, or allow others to do so, for United States Government purposes.

DISCLAIMER

This report was prepared as an account of work sponsored by an agency of the United States Government. Neither the United States Government nor any agency thereof, nor any of their employees, nor any of their contractors, subcontractors, or their employees, makes any warranty, express or implied, or assumes any legal liability or responsibility for the accuracy, completeness, or any third party's use or the results of such use of any information, apparatus, product, or process disclosed, or represents that its use would not infringe privately owned rights. Reference herein to any specific commercial product, process, or service by trade name, trademark, manufacturer, or otherwise, does not necessarily constitute or imply its endorsement, recommendation, or favoring by the United States Government or any agency thereof or its contractors or subcontractors. The views and opinions of authors expressed herein do not necessarily state or reflect those of the United States Government or any agency thereof.

Comparison of hafnium dioxide and zirconium dioxide grown by plasma-enhanced atomic layer deposition for the application of electronic materials

Zhigang Xiao[1*], Kim Kisslinger[2], Sam Chance[1], and Samuel Banks[1]

[1]*Department of Electrical Engineering, Alabama A&M University, Normal, AL 35762*

[2]*Center for Functional Nanomaterials, Brookhaven National Laboratory, Upton, NY 11973*

[*]Corresponding: Tel: 256-372-5679; Fax: 256-372-5855; Email: zhigang.xiao@aamu.edu

Abstract

We report the growth of nanoscale hafnium dioxide (HfO_2) and zirconium dioxide (ZrO_2) thin films using remote plasma-enhanced atomic layer deposition (PE-ALD), and the fabrication of complementary metal-oxide semiconductor (CMOS) integrated circuits using the HfO_2 and ZrO_2 thin films as the gate oxide. Tetrakis (dimethylamino) hafnium ($Hf[N(CH_3)_2]_4$) and Tetrakis (dimethylamino) zirconium (IV) ($Zr[N(CH_3)_2]_4$) were used as the precursors, while O_2 gas was used as the reactive gas. The PE-ALD-grown HfO_2 and ZrO_2 thin films were analyzed using X-ray photoelectron spectroscopy (XPS), X-ray diffraction (XRD), and high-resolution transmission electron microscopy (HRTEM). The XPS measurements show that the ZrO_2 film has the atomic concentrations of 34% Zr, 2% C, and 64% O while the HfO_2 film has the atomic concentrations of 29% Hf, 11% C, and 60% O. The HRTEM and XRD measurements shows both HfO_2 and ZrO_2 films have polycrystalline structures. n-channel and p-channel metal-oxide semiconductor field-effect transistors (nFETs and pFETs), CMOS inverters, and CMOS ring oscillators were fabricated to test the quality of the HfO_2 and ZrO_2 thin films as the gate oxide. Current-voltage (IV) curves, transfer characteristics, and oscillation waveforms were measured from the fabricated transistors, inverters, and oscillators, respectively. The experimental results measured from the HfO_2 and ZrO_2 thin films were compared.

Key words: Hafnium dioxide (HfO_2) thin film; zirconium dioxide (ZrO_2) thin films; complementary metal-oxide semiconductor (CMOS) integrated circuits; CMOS ring oscillator.

I. Introduction

This paper reports the results of remote plasma-enhanced atomic layer deposition (PE-ALD) of nanoscale hafnium dioxide (HfO_2) and zirconium dioxide (ZrO_2) thin films using Tetrakis (dimethylamino) hafnium ($Hf[N(CH_3)_2]_4$) and Tetrakis (dimethylamino) zirconium (IV) ($Zr[N(CH_3)_2]_4$) as the deposition precursors and oxygen as the reactive gas, and the fabrication of complementary metal-oxide semiconductor (CMOS) integrated circuits using the PE-ALD-grown HfO_2 and ZrO_2 as the gate oxide. The objectives were to grow hafnium dioxide (HfO_2) and zirconium dioxide (ZrO_2) thin films at moderate substrate temperatures (200–400 ºC) for the application of high dielectric constant (κ) oxide, to compare the two PE-ALD-grown metal oxides, and to test their functionality and performance as the gate oxide in the fabrication of CMOS integrated circuits.

High-κ metal oxides such as hafnium dioxide (HfO_2) and zirconium dioxide (ZrO_2) thin films have been used as the gate oxide in the fabrication of metal-oxide-semiconductor field-effect transistors (MOSFETs) due to their high dielectric constant (κ) [1-5]. As MOSFETs are scaled down to nanometer sizes, the tunneling currents through the gate dielectrics (the gate leakage current) has become a major concern in today's fabrication of integrated circuits (ICs). High-κ dielectric metal oxide could be a solution to the problem of the gate leakage current. The equivalent oxide thickness (EOT) of the gate dielectric in MOSFETs is: $EOT=(\kappa_{SiO_2}/\kappa)T_{phys}$, where $\kappa_{SiO_2} = 3.9$. An oxide with a higher dielectric constant (κ) has a relatively larger physical thickness (T_{phys}) for an equivalent oxide thickness, thereby lowering the gate leakage current. Hafnium dioxide (HfO_2) and zirconium dioxide (ZrO_2) thin films can be grown using various

techniques, such as physical vapor deposition (PVD) [6, 7], chemical vapor deposition (CVD) [8, 9], plasma-enhanced chemical vapor deposition (PE-CVD) [10, 11], more recently, atomic layer deposition (ALD) [12-18], and plasma-enhanced atomic layer deposition (PE-ALD) [19, 20]. PVD such as sputtering is a clean process without applying chemicals in the process chamber, however, the thin films deposited may have poor conformity. Thermal CVD relies on thermal energy to activate gas-phase and surface reactions. High temperatures between 600 and 1000 ºC are usually required for CVD. Plasma-enhanced chemical vapor deposition (PE-CVD) is an extension of thermal CVD in which gas-phase plasma electron impact is substituted for thermal agitation, thereby achieving much lower substrate temperatures [21-23]. ALD process is similar to the CVD process and uses chemical precursors for the deposition of materials. ALD can produce conformal and ultra-thin films with precise thickness control at the atomic layer level [24-27]. PE-ALD process is similar to the PE-CVD process, and has the advantage of the gas-phase plasma electron impact on the deposition to assist the dissociation of chemicals for active species; therefore, plasma-enhanced ALD can deposit films at much lower temperatures than thermal ALD [28, 29].

There has been extensive research on the growth of metal oxides and their application in the fabricating electronic devices [30-32]. Miniaturization in modern semiconductor industry requires thin film deposition to have atomic level control and the deposited film to be conformal and pinhole-free. The plasma-enhanced atomic layer deposition of HfO_2 and ZrO2 thin films meets the requirement and could be used for the growth of high dielectric constant (κ) gate oxide in the fabrication of integrated circuits (ICs).

II. Experimental Details

Tetrakis (dimethylamino) hafnium ($Hf[N(CH_3)_2]_4$) (TDMAH, 99% purity) and tetrakis (dimethylamino) zirconium (IV) ($Zr[N(CH_3)_2]_4$) (TDMAZ, 99% purity) from the Stream Chemicals, Inc. were used as the precursors, and oxygen was used as reactive gas for the synthesis of the hafnium dioxide (HfO_2) and zirconium dioxide (ZrO_2) thin films. An ALD-150LX system, which was manufactured by the Kurt J. Lesker Company, was used to grow the films. The ALD system comprises a main process chamber, a vacuum load-lock for sample introduction, a remote plasma source and a pumping system. Substrates were loaded into the load lock and transferred to the ALD chamber. The load lock was pumped by a 210 l/s turbo pump backed by a mechanical pump and had a base pressure of 5×10^{-7} Torr. The process chamber was evacuated by a 70 cfm chemical series water-cooled rotary screw dry pump. An inductively coupled remote plasma source (13.56 MHz, 0 – 1000 W) was used to generate high-density plasma for the synthesis of materials in the system. The substrate holder stage was heated at 270 ^{o}C for the deposition of HfO_2 and ZrO_2 films. The precursor bottle for TDMAH was heated at 85 ^{o}C, while the precursor bottle for TDMAZ was heated at 75 ^{o}C. Reactant delivery lines for the delivery of precursors was heated at 100 °C. Carrier gas mass flow controllers (MFC), high-speed ALD valves, and shut off valves were used to control the flow of carrier gas, precursors, and reactant gas into the process chamber. An in-situ ellipsometer (FS-1 multi-wavelength ellipsometer system) was used to monitor the growth of films and perform in-situ measurement of film thickness. The growth rate for both HfO_2 and ZrO_2 film was about 1 Å per cycle (0.04 Å/s) and was confirmed by the HRTEM analysis. The HfO_2 and ZrO_2 thin films were grown in the ALD reactor with a background Ar pressure of about 1.2 Torr and a RF O_2/Ar plasma (100 msec/pulse, 400 Watts, O2:Ar = 3:138 sccm). The HfO_2 and ZrO_2 films, as

the gate oxide in fabricating the CMOS ring oscillators were grown for 100 cycles (~ 10 nm thick). We fabricated 5-stage CMOS ring oscillators to test the quality of the PE-ALD-grown HfO_2 and ZrO_2 film as the gate oxide. A 3-inch-diameter n-type (001) silicon wafer was used in fabricating the complementary metal-oxide semiconductor (CMOS) devices. All the n-channel field-effect transistors (nFETs) in the oscillator had a channel length (L) of about 2 μm, and a channel width (W) of about 6 μm, while all the p-channel field-effect transistor (pFETs) also had a channel length (L) of 2 μm, but a channel width (W) of about 18 μm. The basic fabrication processes included: (1) wet thermal oxidation of silicon wafers for the initial oxide; (2) UV lithography for the patterning in the device fabrication; (3) HF wet etching for etching silicon dioxide; (4) thermal diffusion for boron doping for the fabricating the p-well and the source/drain of pFETs and phosphorous doping for the making the source/drain of nFETs; (5) plasma-enhanced atomic layer deposition of HfO_2 and ZrO_2 thin films for the gate oxide; and, (6) electron beam evaporation of aluminum (Al)/chromium (Cr)/copper (Cu) thin films for the metal contact. For the metallization of devices, we first deposited a metal contact, a 20 nm-thick aluminum (Al) thin film, only on the contact area for the Ohmic contact with silicon, and then overlaid it with a 5 nm-thick chromium (Cr)/100 nm-thick copper (Cu) bilayer film for the final metallization of the device. After the fabrication was completed, we annealed the wafer at 400 ºC under the vacuum of 5×10^{-5} Torr for 20 minutes. Using high-resolution transmission electron microscopy (HRTEM), we analyzed the cross-section morphology and crystalline structure of the HfO_2 and ZrO_2 films and their interface with the silicon substrate. We prepared the TEM samples by the In-situ Lift-out method using a dual-beam FIB (FEI Helios 600 dual beam FIB). The FIB's TEM membranes were imaged in a JEOL 2100F, high-resolution analytical transmission electron microscope at 200 k. X-ray diffraction (XRD) was performed using the

Rigaku Ultima III x-ray diffractometer. X-ray photoelectron spectroscopy (XPS) was performed using the Thermo K-alpha XPS system. The samples were analyzed by XPS as-grown without etching and after an argon ion etching of surface for 30 sec. The surface of HfO_2 and ZrO_2 films was imaged using the FEI Helios 600 dual beam FIB system. The IV curves of nFETs and pFETs and transfer characteristics of CMOS inverters were measured using the Agilent precision source/measurement unit, and the oscillation waveforms of CMOS ring oscillators were measured using the Agilent mixed-signal oscilloscope. To measure the oscillation waveforms from the fabricated 5-stage CMOS ring oscillator, the input of the first CMOS inverter (the first stage) in the oscillator was connected to the output of the fifth CMOS inverter for measuring the oscillation waveform. A voltage of 4 V was applied as the power to the ring oscillators for the electrical measurements. The FS-1 software (Film Sense LLC) was used to analyze the ellipsometric data and determine the refractive index and extinction coefficient of the HfO_2 and ZrO_2 thin film. The FS-1 experimental ellipsometric data were analyzed in the traditional manner, using a parameterized optical model to generate ellipsometric data, and non-linear regression analysis to automatically adjust the model parameters to minimize the difference between the experimental and generated data.

III. Results and Discussion

Table I summarizes the compositions and atomic concentrations, which were obtained by the XPS analysis for the HfO_2 and ZrO_2 thin film grown at the substrate temperature of 270 ^{o}C using the remote plasma-enhanced atomic layer deposition. The HfO_2 film has the atomic concentrations of 17% Hf, 41% C, and 42% O before etching, and 29% Hf, 11% C, and 60% O after the argon ion etching of film surface for 30 sec. The ZrO_2 film has the atomic concentrations of 22% Zr, 27% C, and 51% O before etching, and 34% Zr, 2% C, and 64% O

after the argon ion etching of film surface for 30 sec. The surface of both as-grown HfO_2 and ZrO_2 films has higher concentration of carbon, which is due to being exposed to the atmosphere after removal from the growth chamber. Figure 1(a) and (b) show the XPS survey scan of the HfO_2 thin film grown at the substrate temperature of 270 ºC using the remote plasma-enhanced atomic layer deposition before etching and after etching, respectively. The peak of C 1s after the etching of the film surface is much smaller than that before the etching, which is corresponding to the atomic concentrations before and after the etching in the Table I. Figure 2(a) and (b) show the high-resolution XPS scan of the Hf 4f and O 1s in the HfO_2 thin film, which are compatible with those from the HfO_2 film grown by atomic vapor deposition (AVD) [33]. Figure 3(a) and (b) show the XPS survey scan of the ZrO_2 thin film grown at the substrate temperature of 270 ºC using the remote plasma-enhanced atomic layer deposition before etching and after etching, respectively. After etching of the film surface, no peak of C 1s is visible in the XPS scan, indicating that the ZrO_2 film has a very low concentration of carbon as shown in the Table 1. The possible reason why the ZrO_2 film has a low concentration of carbon is that the precursor of tetrakis (dimethylamino) zirconium (IV) was dissociated well under the argon plasma, making the ZrO_2 film was fully oxidized. Figure 4(a) and (b) show the high-resolution XPS scan of the Zr 3d and O 1s in the Zr O_2 thin film. Figure 5(a) and (b) show the SEM images of the HfO_2 and ZrO_2 films. Both HfO_2 and ZrO_2 films show grain boundaries, while the HfO_2 film has a relatively larger grain size than the ZrO2 film. Figure 6(a) and (b) show the HRTEM images of the cross section of the HfO_2 and ZrO_2 thin films grown on single-crystal silicon wafers. Both films show polycrystalline structures [34]. The HRTEM images also show that a silicon dioxide film of about 3 nm thickness was grown on the silicon substrate initially during the growth of both HfO_2 and ZrO_2 films. Figure 7(a) and (b) show the X-ray diffraction (XRD) spectroscopy of

the HfO_2 and ZrO_2 thin films, respectively. The XRD analysis confirms the polycrystal structures of HfO_2 and ZrO_2 films shown in the HRTEM images in Figure 6(a) and (b). The HfO_2 film has a dominating (-111) crystal orientation [35], while the ZrO2 film has a dominating (111) crystal orientation [36].

Figure 8 show the diffractive index and extinction coefficient of the HfO_2 and ZrO_2 films as a function of wavelength. The optical constants for the HfO_2 and ZrO_2 films are compared in the graph. The diffractive index (n) values for both HfO_2 and ZrO_2 films decrease with increasing wavelength, while the diffractive index (n) values of ZrO_2 film are higher than those of the HfO_2 film. The n values are comparable with those reported by other researchers [35-38]. The extinction coefficient (k) values are quite low (< 0.02) for both films. However, the "k" curve for the HfO_2 film is increasing with increasing wavelength, which is indicative of metallic absorption, which in turn could suggest that the HfO_2 may not be fully oxidized as shown in the XPS analysis, the HfO_2 film has a significant content of carbon. The k curve for HfO_2 film is comparable with that reported in Ref. 39. The "k" curve for the ZrO_2 increases with decreasing wavelength, which is more typical of defect-induced (Urbach) absorption in dielectric films and is comparable with those reported in Ref. 40.

Figure 9 shows a SEM image of a 5-stage CMOS ring oscillator fabricated with the HfO_2 or ZrO_2 as the gate oxide. The ring oscillator consists of 5 CMOS inverters, wherein each inverter consists of an nFET and a pFET. Figure 10(a) and (b) present the drain-source current (I_{DS}) as a function of the drain-source voltage (V_{DS}) and gate voltage (V_{GS}) for the nFET (L=2 μm; W=6 μm) fabricated with HfO_2 and ZrO_2 as the gate oxide, respectively. Figure 11(a) and (b) present

the drain-source current (I_{DS}) as a function of the drain-source voltage (V_{DS}) and gate voltage (V_{GS}) for the pFET (L=2 μm; W=18 μm) with HfO_2 and ZrO_2 as the gate oxide, respectively. Both the nFET and pFET displayed excellent electrical properties of FETs. Figure 12(a) and (b) present the electrical transfer characteristics of a CMOS inverter, which consists of an nFET and a pFET fabricated with HfO_2 and ZrO_2 as the gate oxide, respectively. The applied VDD voltages in the measurement are 3V, 4V, 5V, and 6V. The output voltage decreases sharply from a high voltage (VDD voltage) to a low voltage (GND voltage = 0V) for all the four cases (VDD = 3V, 4V, 5V and 6V), while the input voltage increases to the inverting voltage, indicating that the HfO_2-based and ZrO_2-based CMOS inverters have excellent electrical transfer characteristics and both pFET and nFET in the CMOS inverters functioned very well.

Figure 13(a) an (b) illustrate the oscillation waveforms measured at a VDD voltage of 4V from the CMOS ring oscillators, which were fabricated with HfO_2 and ZrO_2 as the gate oxide, respectively. Both oscillators produce very good rail-to-rail waveforms, following the VDD voltage (4V) and the GND voltage (0V). The oscillator with HfO_2 as the gate oxide has a frequency of 3.8 MHz at the VDD voltage of 4V, while the oscillator with ZrO_2 as the gate oxide has a frequency of 6.2 MHz at the VDD voltage of 4V. The ZrO_2 gate oxide makes the oscillator to oscillate faster than the HfO_2 gate oxide. One possible reason is that ZrO_2 has a higher dielectric constant (ε_r) value ($\varepsilon_r = k^2$) than HfO_2 as shown in Figure 8, higher dielectric constant values made the transistor to switch on and off faster. Another possible reason is that the HfO_2 film is not fully oxidized and has a significate content of carbon as shown in Table I, which may degrade the performance and functionality as the gate oxide.

IV. Summary

Hafnium dioxide (HfO_2) and zirconium dioxide (ZrO_2) thin films were grown at a low substrate temperature (270 ^{o}C) for the application of electronic materials using the remote plasma-enhanced atomic layer deposition (PE-ALD). MOSFETs, CMOS inverters, and CMOS ring oscillators were fabricated with the HfO_2 and ZrO_2 thin films as the gate oxide. The HfO_2 and ZrO_2 thin films were analyzed by the X-ray photoelectron spectroscopy (XPS), high-resolution transmission electron microscopy (HRTEM), and X-ray diffraction (XRD), revealing stoichiometric compositions, polycrystalline structures and good interface with silicon. The nFTTs and pFETs fabricated with the HfO_2 and ZrO_2 thin films as the gate oxide present good current (I)-voltage (V) electrical properties of n-type or p-type field-effect transistors, while the HfO_2- and ZrO_2-based CMOS inverters present good electrical transfer characteristics of inverters. Both the ring oscillators fabricated with the HfO_2 and ZrO_2 thin films as the gate oxide demonstrated satisfactory oscillation waveforms, and the ZrO_2 gate oxide made the oscillator to oscillate faster than the HfO_2 gate oxide. The experimental results measured from the HfO_2 and ZrO_2 films were compared.

Author Contributions

Zhigang Xiao designed the experiments, fabricated the materials and devices, measured the electrical properties of the devices, and wrote the manuscript. Kim Kisslinger performed the HRTEM experiment and contributed to writing the manuscript. Sam Chance performed the fabrication and characterization of the devices. Samuel Banks performed the fabrication and characterization of the devices.

Funding

This research was supported by U.S. Department of Energy, Office of Basic Energy Sciences, under Contract No. DE-SC00112704; National Science Foundation under Grant No. CBET-

1740687; and Department of Defense under Grant No. W911NF-16-1-0554 and W911NF-17-1-0474.

Conflicts of Interest.

The authors declared no conflicts of interest.

Acknowledgements

Research carried out in part at the Center for Functional Nanomaterials, Brookhaven National Laboratory, which is supported by the U.S. Department of Energy, Office of Basic Energy Sciences, under Contract No. DE-SC00112704; the research is supported by National Science Foundation under Grant No. CBET-1740687 and Department of Defense under Grant No. W911NF-16-1-0554 and W911NF-17-1-0474. The authors gratefully thank Dr. Dmytro Nytypanchuk at Brookhaven National Laboratory for help in obtaining the XRD analysis, Dr. Fernando Camino at Brookhaven National Laboratory for help in obtaining the SEM pictures, Ms. Erin C. Prowett at Georgia Institute of Technology for help in obtaining the XPS measurements and analysis, and Mr. Blaine Johs in Film Sense LLC for help in analyzing the refractive index and extinction coefficient of the HfO_2 and ZrO_2 thin films and explaining the data.

References

[1] Wong, H. –S. P. Beyond the conventional transistor. IBM J. Res. & Dev. **2002**, 46, 133-168.

[2] Robertson, J. High dielectric constant gate oxides for metal oxide Si transistors. Rep. Prog. Phys. **2006**, 69, 327-396.

[3] Robertson, J. & Wallace, R. M. High-K materials and metal gates for CMOS applications. Mater. Sci. Eng. **2005**, R88, 1-41.

[4] Al-Kuhaili, M. F., Durrani, S. M. A. & Khawaja, E. E. Characterization of hafnium oxide thin films prepared by electron beam evaporation. J. Phys. D: Appl. Phys. **2004**, 37, 1254-1261.

[5] Smith, R. C., Ma, T., Hoilien, N., Tsung, L. Y., Bevan, M. J., Colombo, L., Roberts, J., Campbell, S. A. & Gladfelter, W. L. Chemical vapour deposition of the oxides of titanium, zirconium and hafnium for use as high-k materials in microelectronic devices. A carbon-free precursor for the synthesis of hafnium dioxide. Adv. Mater. Opt. Electron. **2000**, 10, 105-114.

[6] Lee, U. S., Choi, J. S., Yang, B. S., Oh, S., Kim, Y. J., Oh, M. S., Heo, J. & Kima, H. J. Formation of a bilayer of ALD-SiO_2 and sputtered Al_2O_3/ZrO_2 films on polyethylene terephthalate substrates as a moisture barrier. *ECS* Solid State Lett. **2013**, 2, R13-R15.

[7] Venkataraj, S., Kappertz, O., Weis, H., Drese, R., Jayavel, R., & Wuttig, M. Structural and optical properties of thin zirconium oxide films prepared by reactive direct current magnetron sputtering. J. Appl. Phys. **2002**, 92, 3599-3607.

[8] Chang, J. P., Lin, Y. S., & Chu, K. Rapid thermal chemical vapor deposition of zirconium oxide for metal-oxide semiconductor field effect transistor application. J. Vac. Sci. Technol. B **2001**, 19, 1782-1787.

[9] Nienow, A. M. & Roberts, J. T. Chemical vapor deposition of zirconium oxide on aerosolized silicon nanoparticles. Chem. Mater. **2006**, 18, 5571-5577.

[10] Choi, K. J., Shin, W. C. & Yoon, S. G. Ultrathin HfO_2 gate dielectric grown by plasma-enhanced chemical vapor deposition using $Hf[OC(CH_3)_3]_4$ as a precursor in the absence of O_2. J. Mater. Res. **2003**, 18, 60-65.

[11] Katoa, H., Nango, T., Miyagawa, T., Katagiri, T., Seol, K. S. & Ohki, Y. Plasma-enhanced chemical vapor deposition and characterization of high-permittivity hafnium and zirconium silicate films. J. Appl. Phys. **2002**, 92, 1106-1111.

[12] McNeill, D. W., Bhattacharya, S., Wadsworth, H., Ruddell, F. H., Mitchell, S. J. N., Armstrong, B. M., & Gamble, H. S. Atomic layer deposition of hafnium oxide dielectrics on silicon and germanium substrates. J. Mater. Sci.: Mater. Electron. **2008**, 19, 119.

[13] Senzaki, Y., Park, S., Chatham, H., Bartholomew, L., & Nieveen, W. Physical and electrical characterization of Ce-HfO_2 thin films deposited by thermal atomic layer deposition. J. Vac. Sci. Technol. A **2004**, 22, 1175-1181.

[14] Hausmann, D. M., Kim, E., Becker, J. & Gordon, R. G. Atomic layer deposition of hafnium and zirconium oxides using metal amide precursors. Chem. Mater. **2002**, 14, 4350-4358.

[15] Nomura, K., Ohta, H., Ueda, K., Kamiya, T., Hirano, M. & Hosono, H. Thin-film transistor fabricated in single-crystalline transparent oxide semiconductor. Science **2003**, 300, 1269-1272.

[16] Cheynet, M. C., Pokrant, S., Tichelaar, F. D. & Rouviere, J. L. Crystal structure and band gap determination of HfO_2 thin films. J. Appl. Phys. **2007**, 101, 054101-054108.

[17] Bohra, F., Jiang, B. & Zuo, J. M. Textured crystallization of ultrathin hafnium oxide films on silicon substrate. Appl. Phys. Lett. **2007**, 90, 161917-1-161917-3.

[18] Kim, H., Mclntyre, P. C. & Saraswat, K. C. Effects of crystallization on the electrical properties of ultrathin dielectrics grown by atomic layer deposition. Appl. Phys. Lett. **2003**, 82, 106-108.

[19] Lao, S. X., Martin, R. M. & Chang, J. P. Plasma enhanced atomic layer deposition of HfO_2 and ZrO_2 high-k thin films. J. Vac. Sci. Technol. A **2005**, 23, 488-496.

[20] Jung, H., Oh, I. K., Yoon, C. M., Park, B. E., Lee, S., Kwon, O., Lee, W. J., Kwon, S. H., Kim, W. H. & Kim, H. Effects of Ar addition to O_2 plasma on plasma-enhanced atomic layer deposition of oxide thin films. ACS Appl. Mater. Interfaces **2018**, 10, 40286−40293.

[21] Xiao, Z. & Mantei, T. D. Deposition of hard metal nitride-like coatings in an electron cyclotronresonance discharge. Surf. Coat. Technol. **2004**, 177–178, 389–393.

[22] Xiao, Z. & Mantei, T. D. Plasma-assisted growth of bilayer silicon-containing coatings for hardness and corrosion resistance. J. Vac. Sci. Technol. A **2004**, 22, 1124-1128.

[23] Xiao, Z. Robust and inexpensive thermal vaporizer for low-vapor pressure liquids. Rev. Sci. Instrum. **2003**, 74, 3879-3880.

[24] George, S. M. Atomic layer deposition: An overview. Chem. Rev. **2010**, 110, 111–131.

[25] McDaniel, M. D., Ngo, T. Q., Hu, S., Posadas, A., Demkov, A. A., & Ekerdt, J. G. Atomic layer deposition of perovskite oxides and their epitaxial integration with Si, Ge, and other semiconductors. Appl. Phys. Rev. **2015**, 2, 041301-1-32.

[26] Motamedi, P. & Cadienn, K. Structural and optical characterization of low-temperature ALD crystalline AlN. J. Cryst. Growth **2015**, 421, 45–52.

[27] Johnson, R. W., Hultqvist, A. & Stacey, F. B. A brief review of atomic layer deposition: from fundamentals to applications. Materials Today **2014**, 17, 236-246.

[28] Profijt, H. B., Potts, S. E., van de Sanden, M. C. M. & Kesselsa, W. M. M. Plasma-assisted atomic layer deposition: basics, opportunities, and challenges, J. Vac. Sci. Technol. A **2011**, 29, 050801-1-050801-26.

[29] Zhang, Y., Ren, W., Jiang, Z. Yang, S., Jing, W., Shi, P., Wu, X. & Ye, Z. G. Low-temperature remote plasma-enhanced atomic layer deposition of graphene and characterization of its atomic-level structure. J. Mater. Chem. C **2014**, 2, 7570–7574.

[30] Huang, R. G., Tham, D., Wang, D., & Heath, J. R. High performance ring oscillators from 10-nm wide silicon nanowire field-effect transistors. Nano Res. **2011**, 4, 1005-1012.

[31] Wang, H., Yu, L., Lee, Y. H., Shi, Y., Hsu, A., Chin, M. L., Li, L. J., Dubey, M., Kong, J. & Palacios, T. Integrated circuits based on bilayer MoS_2 transistors. Nano Lett. **2012**, 12, 4674-4680.

[32] Xiao, Z. & Kisslinger, K. Electron-beam-evaporated thin films of hafnium dioxide for fabricating electronic devices. J. Vac. Sci. Technol. B **2015**, 33, 042001-1- 042001-4.

[33] Luo, X.; Li, Y.; Yang, H.; Liang, Y.; He, K.; Sun, W.; Lin, H.; Yao, S.; Lu, X.; Wan, L.; Feng, Z. Investigation of HfO_2 thin films on Si by X-ray photoelectron spectroscopy, Rutherford backscattering, grazing incidence X-ray diffraction and variable angle spectroscopic ellipsometry. Crystals **2018**, 8, 248.

[34] Houska J. Molecular dynamics study of the growth of crystalline ZrO_2. Surf. Coat. Technol. **2016**, 304, 23-30.

[35] Ramzan, M.; Wasiq, M. F.; Rana, A.M.; Ali, S.; Nadeem, M. Y. Characterization of e-eam evaporated hafnium oxide thin films on post thermal annealing. Appl. Surf. Sci. **2013**, 283, 617-622.

[36] Zhao, Z. W.; Tay, B. K.; Huang, L.; Yu, G. Q. Study of the structure and optical properties of nanocrystalline zirconium oxide thin films deposited at low temperatures. J. Phys. D: Appl. Phys. **2004**, 37, 1701-1705.

[37] Vicek, J.; Belosludtsev A.; Rezek, J.; Houska, J.; Capek, J.; Cerstvy, R.; Haviar, S. High-rate reactive high-power impulse magnetron sputtering of hard and optically transparent HfO_2 films. Surf. Coat. Technol. **2016**, 290, 58-64.

[38] Vicek, J.; Rezek, J.; Houska, J.; Kozak, T.; Kohout, J. Benefits of the controlled reactive high-power impulse magnetron sputtering of stoichiometric ZrO_2 films. Vacuum **2015**, 114, 131-141.

[39] Ramzan, M.; Rana, A. M.; Ahmed, E.; Wasiq, M. F.; Bhatti, A. S.; Hafeez, M.; Ali, A.; Nadeem, M. Y. Optical characterization of hafnium oxide thin films for heat mirrors. Mater. Sci. Semi. Pro. **2015**, 32, 22-30.

[40] Sidqi, N.; Clark, C.; Buller, G. S.; Krishna, G.; Thalluri, V. V.; Mitrofanov, J.; Noblet, Y. Comparative study of dielectric coating materials for micro-cavity applications. Opt. Mater. Expr. **2019**, 9, 3452-3468.

Figure Captions:

Fig. 1. (a) XPS survey scan of the HfO_2 thin film before etching; (b) XPS survey scan of the HfO_2 thin film after etching.

Fig. 2. (a) High-resolution XPS scan of the Hf 4f in the HfO_2 film; (b) High-resolution XPS scan of the O 1s in the HfO_2 film.

Fig. 3. (a) XPS survey scan of the ZrO_2 thin film before etching; (b) XPS survey scan of the ZrO_2 thin film after etching.

Fig. 4. (a) High-resolution XPS scan of the Zr 3d in the ZrO_2 film; (b) High-resolution XPS scan of the O 1s in the ZrO_2 film.

Fig. 5. (a) SEM image of the HfO_2 thin film; (b) SEM image of the ZrO_2 thin film.

Fig. 6. (a) HRTEM image of the cross section of the HfO_2 thin film; (b) HRTEM image of the cross section of the ZrO_2 thin film.

Fig. 7. (a) XRD spectroscopy of the HfO_2 thin film; (b) XRD spectroscopy of the ZrO_2 thin film.

Fig. 8. Refractive index and extinction coefficient of the HfO_2 and ZrO_2 thin films versus wavelength.

Fig. 9. SEM image of a CMOS ring oscillator fabricated with HfO_2 or ZrO_2 as the gate oxide.

Fig. 10. (a) Drain-source current (I_{DS}) versus drain-source voltage (V_{DS}) and gate voltage (V_{GS}) for the nFET fabricated with the HfO_2 thin film as the gate oxide; (b) Drain-source current (I_{DS}) versus drain-source voltage (V_{DS}) and gate voltage (V_{GS}) for the nFET fabricated with the ZrO_2 thin film as the gate oxide.

Fig. 11. (a) Drain-source current (I_{DS}) versus drain-source voltage (V_{DS}) and gate voltage (V_{GS}) for the pFET fabricated with the HfO_2 thin film as the gate oxide; (b) Drain-source current (I_{DS})

versus drain-source voltage (V_{DS}) and gate voltage (V_{GS}) for the pFET fabricated with the ZrO_2 thin film as the gate oxide.

Fig.12. (a) Transfer characteristics of the CMOS inverter fabricated with the HfO_2 thin film as the gate oxide; (b) Transfer characteristics of the CMOS inverter fabricated with the ZrO_2 thin film as the gate oxide.

Fig. 13. (a) the oscillation waveform of the HfO_2-based CMOS ring oscillator at the VDD voltage of 4V; (b) the oscillation waveform of the ZrO_2-based CMOS ring oscillator at the VDD voltage of 4V

Table I. Compositions of HfO_2 and ZrO_2 films measured by XPS before and after etching

	Atomic Concentration (%) of HfO_2 film			Atomic Concentration (%) of ZrO_2 film		
	Hf	C	O	Zr	C	O
Before Etching	17	41	42	22	27	51
After Etching	29	11	60	34	2	64

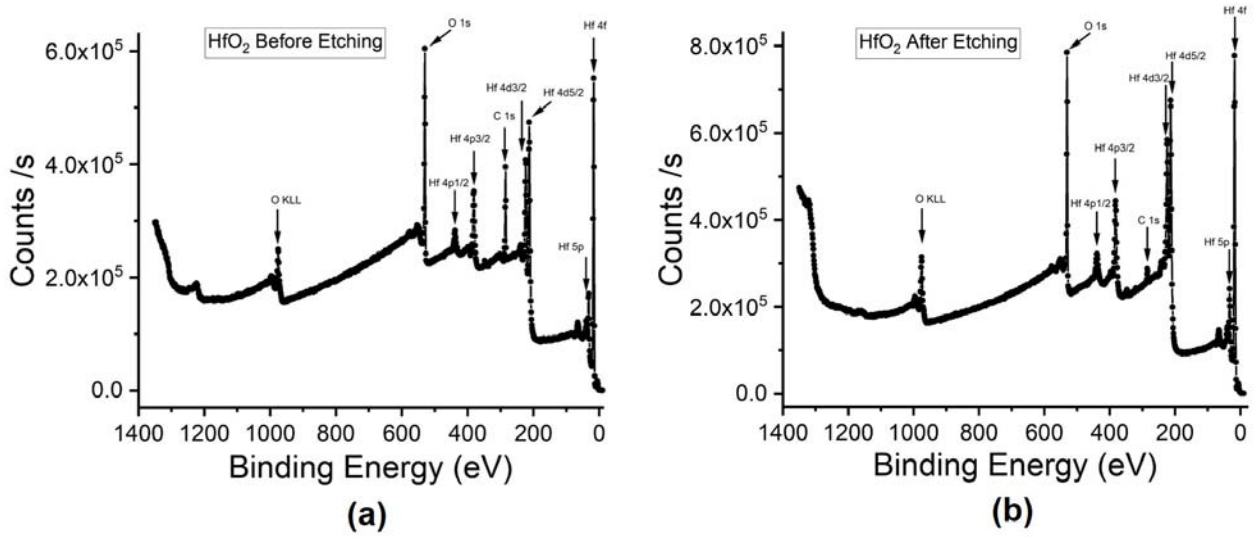
HfO2 Before Etching
O 1s
Hf 4f
Hf 4d3/2
Hf 4d5/2
C 1s
Hf 4p3/2
Hf 4p1/2
O KLL
Hf 5p
Counts /s
6.0x10^5
4.0x10^5
2.0x10^5
0.0
1400 1200 1000 800 600 400 200 0
Binding Energy (eV)
(a)
HfO2 After Etching
O 1s
Hf 4f
Hf 4d5/2
Hf 4d3/2
Hf 4p3/2
Hf 4p1/2
C 1s
O KLL
Hf 5p
Counts /s
8.0x10^5
6.0x10^5
4.0x10^5
2.0x10^5
0.0
1400 1200 1000 800 600 400 200 0
Binding Energy (eV)
(b)

Fig. 1

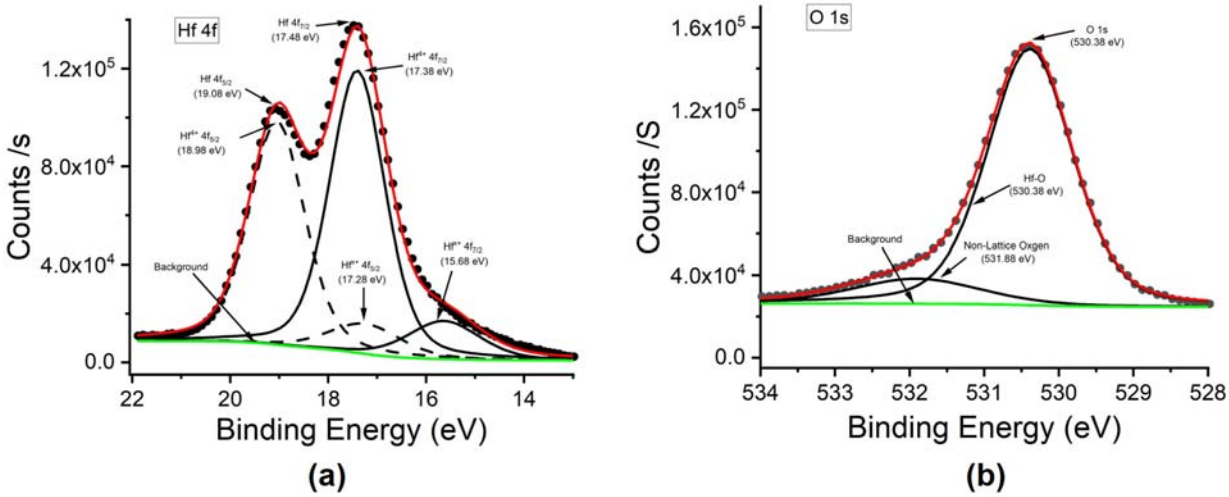
Hf 4f
Hf 4f7/2 (17.48 eV)
Hf4+ 4f7/2 (17.38 eV)
Hf 4f5/2 (19.08 eV)
Hf4+ 4f5/2 (18.98 eV)
Background
Hf** 4f7/2 (17.28 eV)
Hf** 4f7/2 (15.68 eV)
Counts /s
1.2x10^5
8.0x10^4
4.0x10^4
0.0
22
20
18
16
14
Binding Energy (eV)
(a)
O 1s
O 1s (530.38 eV)
Hf-O (530.38 eV)
Background
Non-Lattice Oxgen (531.88 eV)
Counts /S
1.6x10^5
1.2x10^5
8.0x10^4
4.0x10^4
0.0
534
533
532
531
530
529
528
Binding Energy (eV)
(b)

Fig. 2

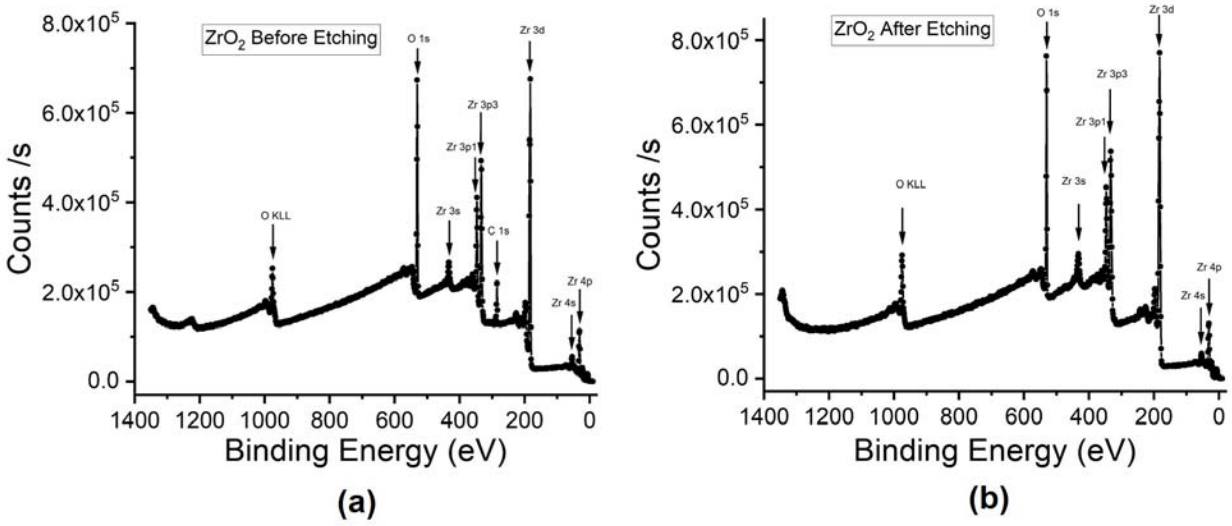
ZrO2 Before Etching
O 1s
Zr 3d
Zr 3p3
Zr 3p1
Zr 3s
C 1s
O KLL
Zr 4p
Zr 4s
Counts /s
Binding Energy (eV)
(a)
ZrO2 After Etching
O 1s
Zr 3d
Zr 3p3
Zr 3p1
Zr 3s
O KLL
Zr 4p
Zr 4s
Counts /s
Binding Energy (eV)
(b)

Fig. 3

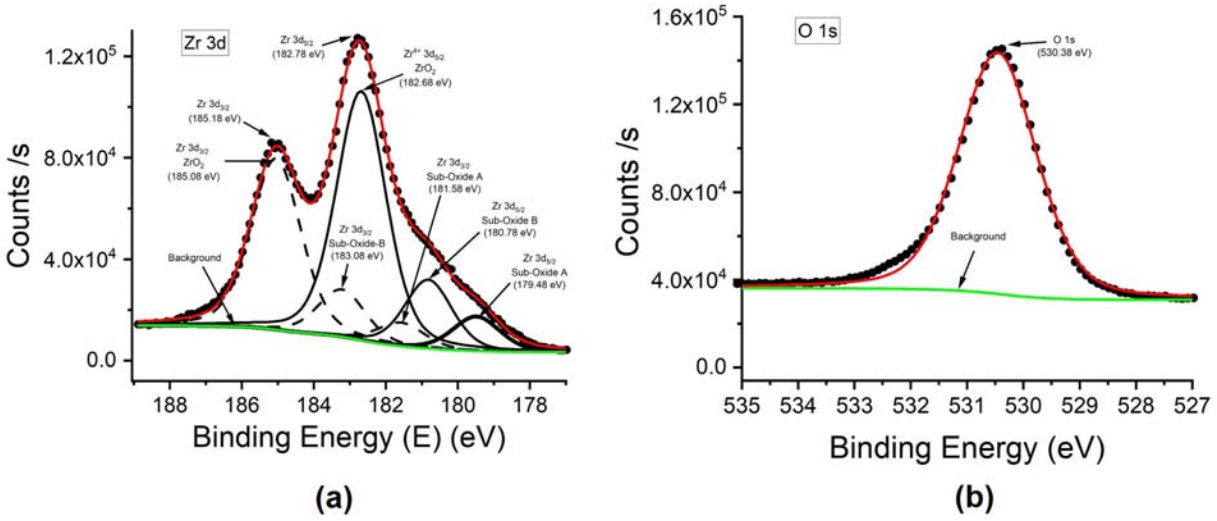
Zr 3d
Zr 3d5/2 (182.78 eV)
Zr4+ 3d3/2 ZrO2 (182.68 eV)
Zr 3d3/2 (185.18 eV)
Zr 3d3/2 ZrO2 (185.08 eV)
Zr 3d3/2 Sub-Oxide A (181.58 eV)
Zr 3d3/2 Sub-Oxide B (180.78 eV)
Zr 3d3/2 Sub-Oxide-B (183.08 eV)
Zr 3d5/2 Sub-Oxide A (179.48 eV)
Background
Counts /s
Binding Energy (E) (eV)
(a)
O 1s
O 1s (530.38 eV)
Background
Counts /s
Binding Energy (eV)
(b)

Fig. 4

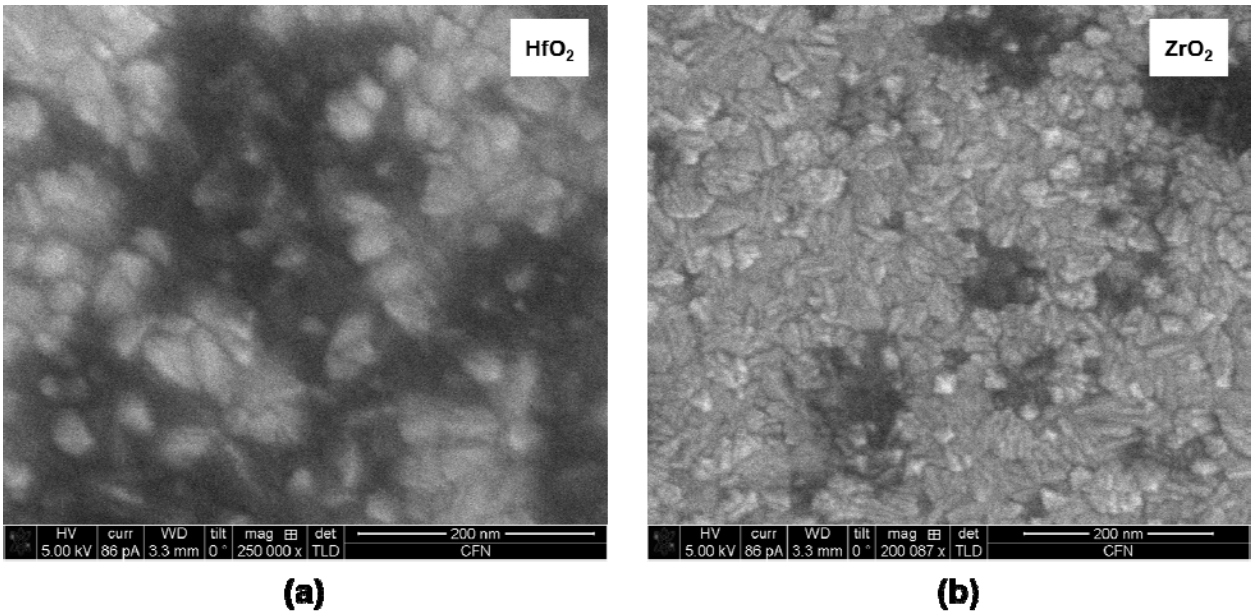
HfO2
HV 5.00 kV
curr 86 pA
WD 3.3 mm
tilt 0 °
mag 250 000 x
det TLD
200 nm
CFN
ZrO2
HV 5.00 kV
curr 86 pA
WD 3.3 mm
tilt 0 °
mag 200 087 x
det TLD
200 nm
CFN

(a) **(b)**

Fig. 5

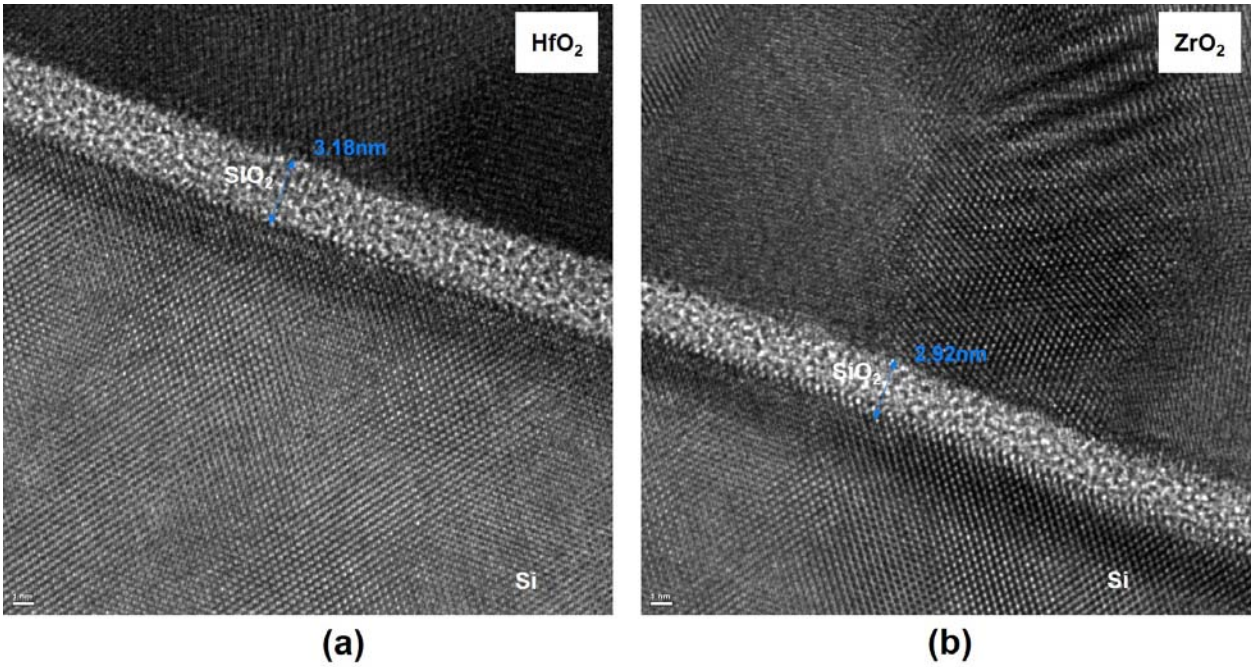

Fig. 6

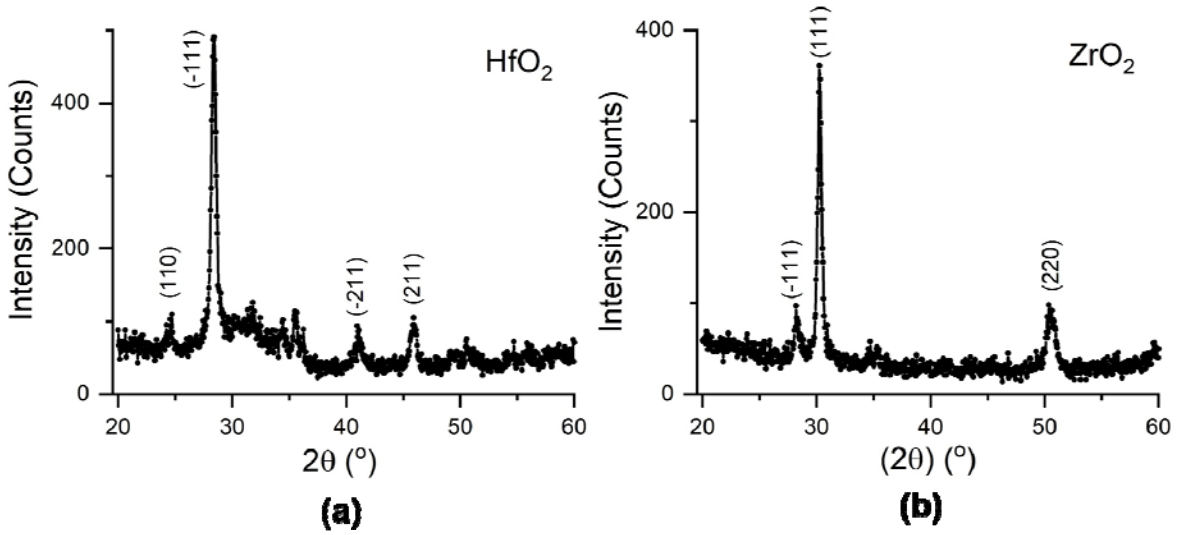
HfO2
Intensity (Counts)
400
200
0
(110)
(-111)
(-211)
(211)
20
30
40
50
60
2θ (°)
(a)
ZrO2
Intensity (Counts)
400
200
0
(-111)
(111)
(220)
20
30
40
50
60
(2θ) (°)
(b)

Fig. 7

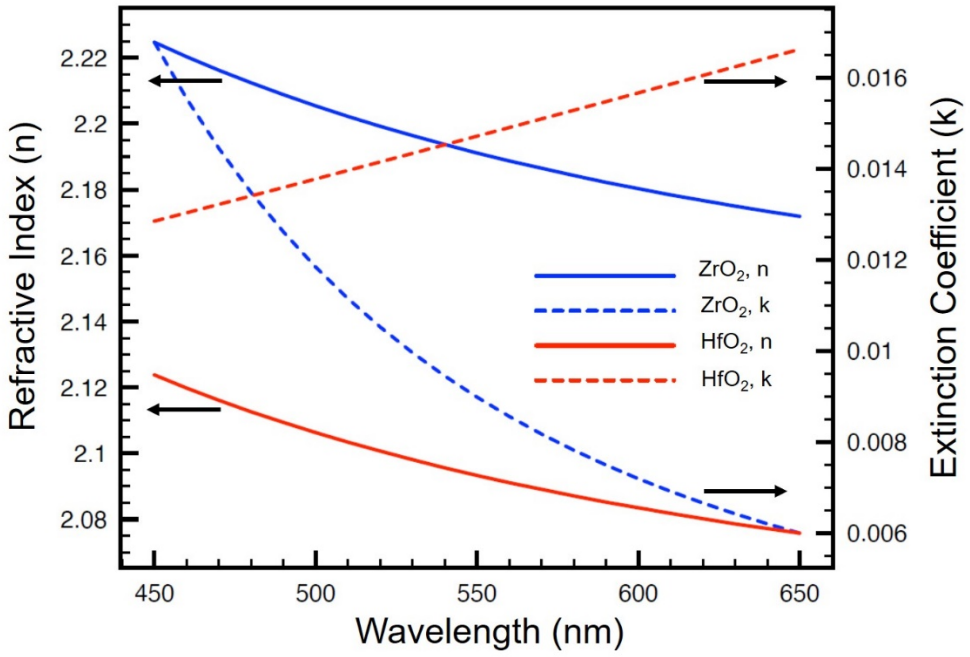
Refractive Index (n)
Extinction Coefficient (k)
Wavelength (nm)
2.22
2.2
2.18
2.16
2.14
2.12
2.1
2.08
0.016
0.014
0.012
0.01
0.008
0.006
450
500
550
600
650
ZrO2, n
ZrO2, k
HfO2, n
HfO2, k

Fig. 8

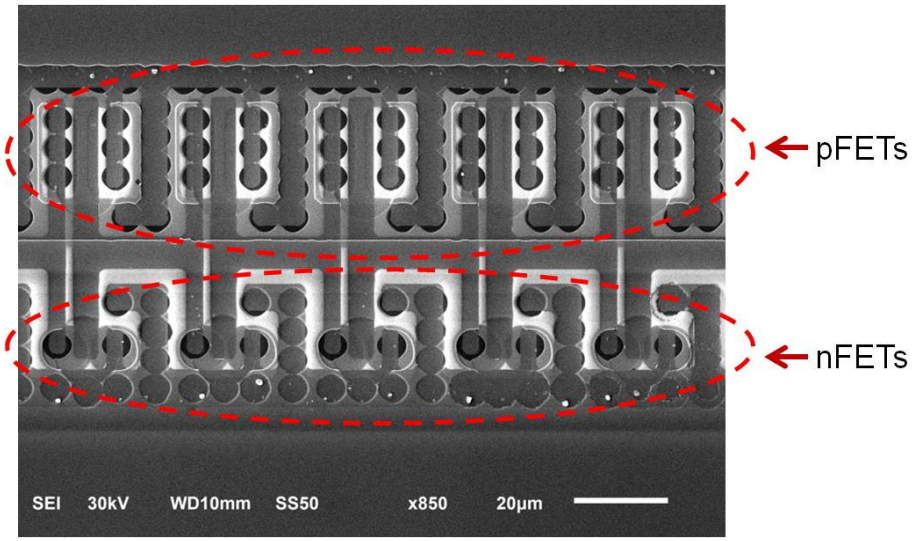
pFETs
nFETs
SEI 30kV WD10mm SS50 x850 20μm

Fig. 9

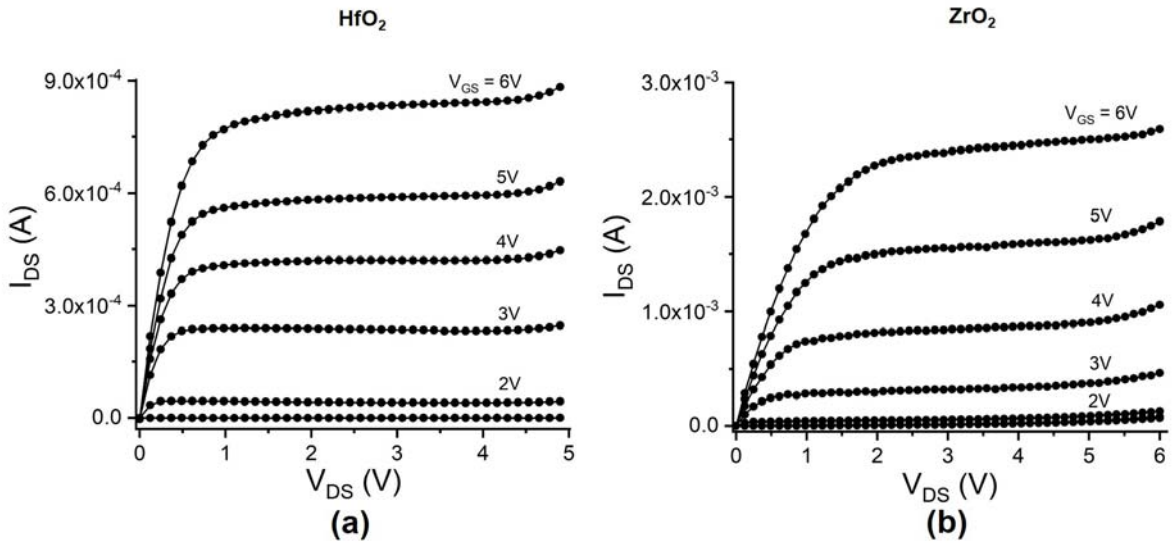
HfO2
ZrO2
9.0x10-4
6.0x10-4
3.0x10-4
0.0
IDS (A)
VGS = 6V
5V
4V
3V
2V
0
1
2
3
4
5
VDS (V)
(a)
3.0x10-3
2.0x10-3
1.0x10-3
0.0
IDS (A)
VGS = 6V
5V
4V
3V
2V
0
1
2
3
4
5
6
VDS (V)
(b)

Fig. 10

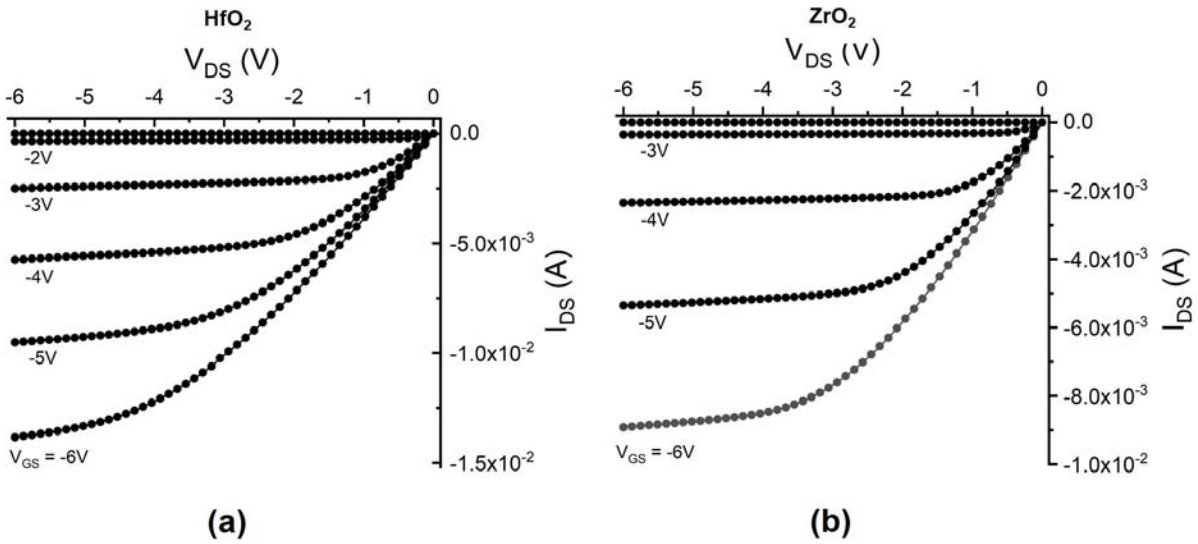
HfO2
VDS (V)
-6 -5 -4 -3 -2 -1 0
0.0
-5.0x10-3
-1.0x10-2
-1.5x10-2
IDS (A)
-2V
-3V
-4V
-5V
VGS = -6V
(a)
ZrO2
VDS (V)
-6 -5 -4 -3 -2 -1 0
0.0
-2.0x10-3
-4.0x10-3
-6.0x10-3
-8.0x10-3
-1.0x10-2
IDS (A)
-3V
-4V
-5V
VGS = -6V
(b)

Fig. 11

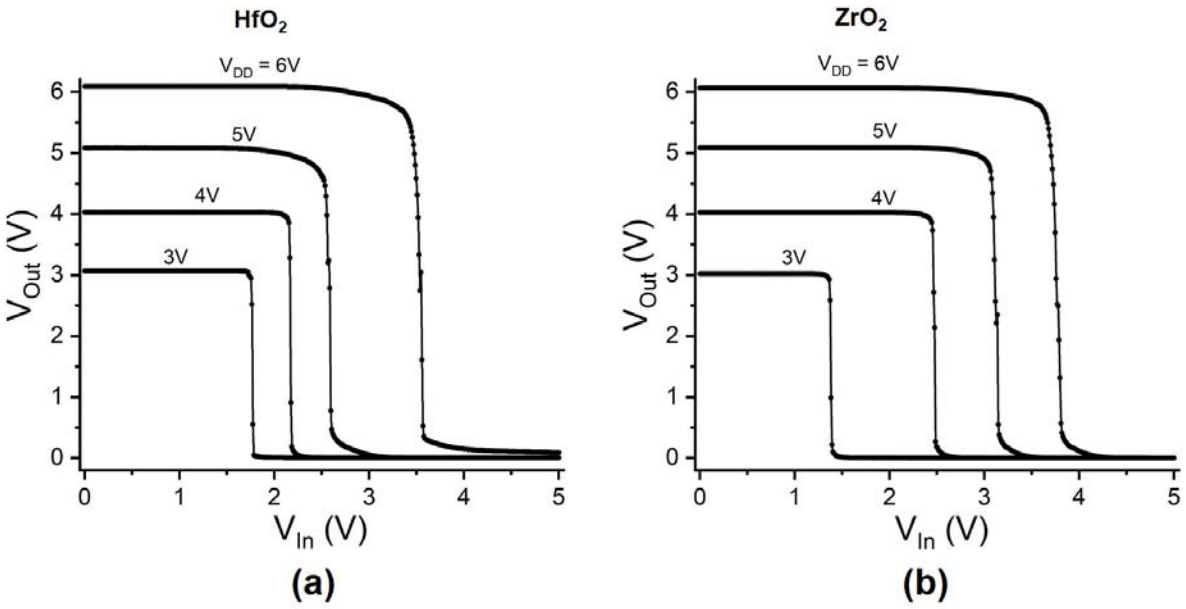
HfO2
VDD = 6V
5V
4V
3V
VOut (V)
VIn (V)
(a)
ZrO2
VDD = 6V
5V
4V
3V
VOut (V)
VIn (V)
(b)

Fig. 12

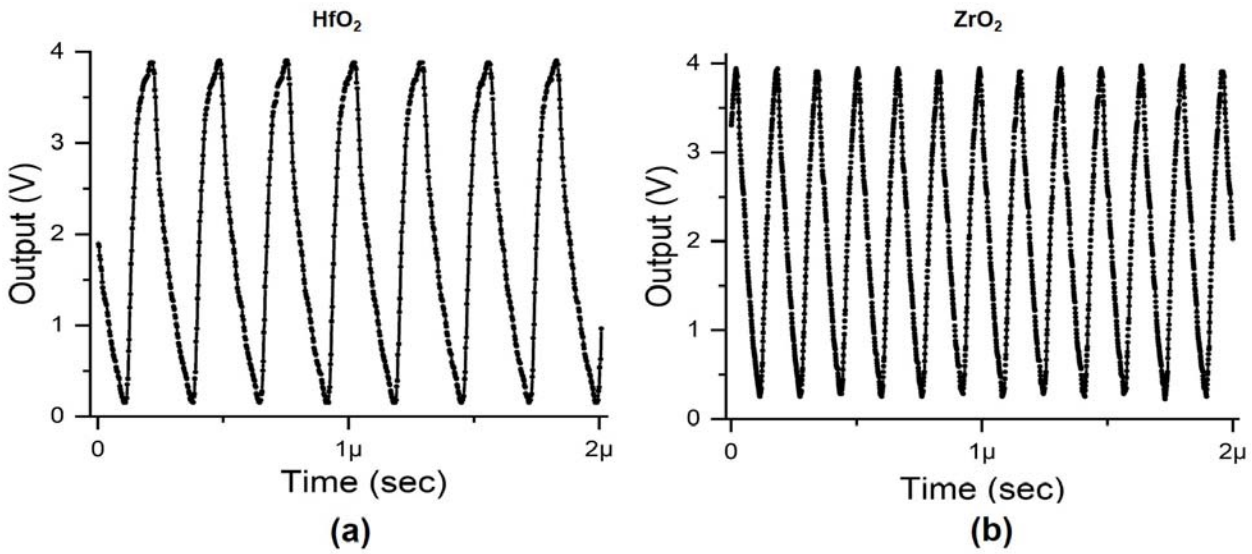

Fig. 13